

LABORATORY INVESTIGATIONS ON CONCRETE FRACTURE USING ACOUSTIC EMISSION TECHNIQUE

R.VIDYA SAGAR^{*}, B.K.RAGHU PRASAD[†] R.K.SINGH[#]

^{*}Department of Civil Engineering
Indian Institute of Science, Bangalore 560 012, India
e-mail: rvsagar@civil.iisc.ernet.in

[†]Advisor
Indian Institute of Science, Bangalore 560 012, India
e-mail: bkr@civil.iisc.ernet.in

[#]Reactor Safety Division,
Engg. Hall-7,
Bhabha Atomic Research Centre,
Trombay, Mumbai 400085, India
e-mail: rksingh@barc.gov.in

Key words: Fracture, Reinforced Concrete, Acoustic emission

Abstract: Acoustic emission (AE) monitoring studies have been carried out under controlled laboratory conditions on plain concrete beams and reinforced concrete (RC) beams. The results of AE statistics have revealed interesting features of the various stages of stress induced micro-fracturing and growth leading to the failure of plain concrete beams and RC beams. The experimental details, results and their applications are presented in this article.

1 INTRODUCTION

Understanding the mechanism of concrete fracture at the laboratory scale under simulated field conditions as well as *in situ* is a subject of interest in the discipline of fracture mechanics of concrete structures. It is known that failure of concrete occurs due to the formation and growth of stress induced micro-cracks. Micro-cracking is accompanied by the release of stored strain energy in the form of AE. There are different mechanisms by which micro-cracks initiate and grow and later coalesce to form macro cracks in concrete structures [1-4]. But the important tasks are to detect, characterize and locate the damage also evaluate the criticality (or state of damage), so that adequate steps can be taken to control and prevent the failure in concrete structures. Another important task is to evolve

technologies for earthquake prediction based AE research and concrete fracture mechanics principles. In order to meet such requirements, elaborate research work has been carried out in the recent years on the development and application of AE monitoring and analytical techniques [6-10]. At the laboratory scale, simultaneous and accurate monitoring and recording of stress induced AE data of a concrete structure under different loading conditions have been possible [9-10].

A few laboratory experiments have been performed on RC beams and plain concrete beams for the study of concrete fracture using AE techniques. Nine RC beams with three different span-to-depth ratios ranging from 2.0 to 6.0 with a reinforcement ratio roughly kept the same (1.4to1.5%) were tested under bending till failure and simultaneously the

released AE was recorded. The criteria used to characterize the cracking in RC beams are based on the AE parameters. The variation of AE parameters during different stages of cracking was noticed. AE parameters such as frequency, duration, amplitude, count, rise time, parameters depend on AE signatures such as b-value and damage parameter(D), follow the fracture process during the entire loading. The results are useful to distinguish different cracks in RC beams and extend them for field applications.

2. AE PARAMETER ANALYSIS

It is known that macro-cracks are visible to human eye and on the other hand micro-cracks are not visible to human eye. The advantage about AE technique is that the damage state can be related to AE signatures. In case of real structures, where damage of similar magnitude cannot be easily identified visually, where, analysis of the damage can be assessed using AE parameters. Thus, it is important to identify and estimate the damage of RC structures using the AE parameters. AE parameters such as amplitude, average frequency, rise time, RA value and maximum RMS are useful in characterizing the damage in RC structures, and can be used for field conditions. AE parametric analysis was used by earlier researchers to characterize the cracking mode in laboratory conditions using RC specimens [12-15]. Figure 1 shows a typical AE signal and the corresponding AE parameters.

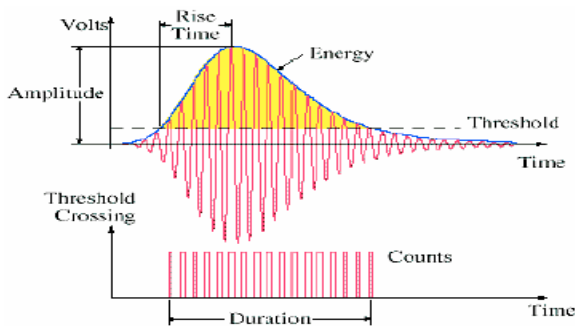


Figure 1: A typical Acoustic emission signal and the corresponding AE parameters

One of the important parameter which is

influenced by the mode of cracking is the average frequency (AF) defined as given below[9]

$$\text{Average Frequency (AF)} = \frac{\text{AE counts}}{\text{duration}} \quad (1)$$

measured in kHz. AF estimates the frequency content of the waveform. RA value is another AE parameter defined as given below [5,11].

$$\text{RA} = \frac{\text{Rise time (RT)}}{\text{Amplitude}} \quad (2)$$

2.1 AE based b-value:

In seismology, *b*-value is defined as the negative slope of the plot between logarithm of earthquake frequency and its magnitude. In general *b*-value is computed using cumulative frequency-magnitude data by applying Gutenberg-Richter relationship used in seismology [15]. In context of AE technique, the Gutenberg- Richter relationship is given by [21]

$$\log_{10} N(M) = a - b \left(\frac{A_{dB}}{20} \right) \quad (4)$$

A_{dB} is the peak amplitude of AE events in dB and N is the incremental frequency that the number of AE hits with amplitude greater than the threshold, 'a' is an empirical constant and b is the AE based *b*-value. Equation (4) is based on fact that AE events of larger magnitude occur less frequently than events of smaller magnitude. The amplitude value has to be divided by a factor of 20 in order to get *b*-values comparable to seismic values [21].

2.3 Damage Parameter (D)

Cox and Meredith (1993) derived a parameter (D) to assess the microcracks in rock under compression. The accumulated state of damage is given by [22-23]

$$D = \sum 10^{cm} \quad (5)$$

Where m is seismic magnitude and c is a constant and it is equal to 3. the constant c depends on the type of the instrument used in the experiment. The constant m computed here is the AE event amplitude in dB/20.

3 AIM OF THE PRESENT STUDY

Interpretation of cracks in RC structures is

useful for the extension of its service life so that a necessary and required action can be taken. Generally in RC structures flexural cracks, shear cracks and interface cracks develop. In order to rehabilitate the RC structure which is already under service, it is needed to understand whether it is to be strengthened in flexure or in shear. There are many methods to strengthen a structure based on the cause of crack. Improvement of bond characteristics between coarse aggregate and cement matrix is done if interface cracks are observed. Similarly, various methods like additional longitudinal reinforcement steel jackets, carbon fiber jackets and extra web reinforcements in the form of steel/ carbon fiber/ glass fiber wrapping are also used to strengthen the structure. In order to use the appropriate method of strengthening, one needs to know whether the member under consideration is weakened due to flexure or shear respectively. Although classification of cracks in concrete structures was studied earlier by using AE technique, the authors in the present experimental study gave emphasis on the variation of AE parameters during the development of tensile/flexure and shear cracks [5,11,12,24-25] in RC beams during bending. The aim of the present experimental study is to know about the variation of AE parameters during cracking in RC beams subjected to bending in laboratory conditions.

4 EXPERIMENTAL PROGRAM

4.1 Specimens

A set of 9 RC beams of three different depths viz., 150 mm, 300 mm and 450 mm with rectangular cross section were tested and the geometric details of these specimens are given in Table 1. Also three point bend specimen made with plain concrete [78 MPa and 50 MPa] and cement mortar were tested under CMOD control with 0.004 mm/sec rate of loading. An electrical strain gauge was affixed to the main reinforcing bar before casting to measure the strain in steel at mid-section of the specimen.

4.2 Materials

The materials used for the present study are

cement, fine aggregate, coarse aggregate (maximum size 20 mm). The details of concrete mixture are summarized in Table 2. Along with test specimens, cubes and cylinders were also cast for compressive strength determination. After casting, the specimen demoulding was carried out with a time gap of 24 hours. The 28th day compressive strength of concrete mixture is 58 MPa and tensile strength is 3.5 MPa.

4.3 Test set setup

The experimental set up consisted of a servo-hydraulic loading frame with a data acquisition system and an AE monitoring system. The data acquisition system records load, displacement, strain in steel and time. A steel I-beam was placed as a spreader beam beneath the actuator to transfer as two point loads as shown in Figure 2. Displacement of the beam was measured at three locations at centre of the specimen, 1m from left and right supports using a linear variable differential transformer (LVDT), placed on the underside of the specimen.

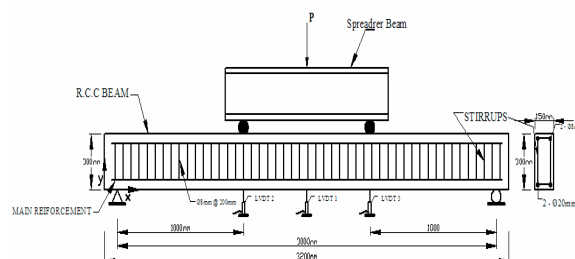


Figure 2. Schematic diagram of test specimen

The AE instrument is a 8 channel AEwin SAMOS (Sensor based Acoustic Multi-channel Operating System) E2.0 system which was used in the present study. The AE setup consisted of AE sensors, pre-amplifiers and an AE data recording system. The transducers (sensors) used in the experimental study were R6D resonant type (PAC make). The diameter of AE sensor is 19.0 mm and its height is 22.0 mm. The AE transducers has peak sensitivity at -75 dB with reference 1V/ (m/s). The operating frequency of the AE sensor is 35 kHz – 100 kHz. The output of a differential sensor is processed by a differential amplifier.

AE signals over 40 dB were recorded as AE waves with AE parameters. The AE acquisition system records AE event parameters.

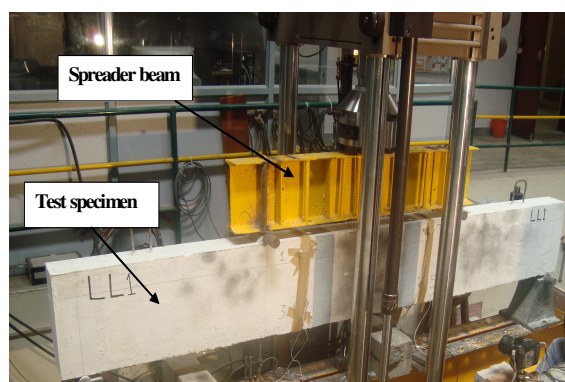


Figure 3: RC beam specimen in the test rig, structures lab, department of civil engineering, Indian Institute of Science, Bangalore , India.

Vacuum grease LR (high vacuum silicon grease) was used as a coupling agent to the sensor and the surface of the test specimen and the sensors were secured by the use of a tape during the experiment. The AE signals were recorded in eight-channel monitoring board PCI-8, with a sampling rate of 5 MHz. The location of AE sensors on the test specimen is given in Table 3.

5. RESULTS AND DISCUSSION

Figure 3 shows a RC beam specimen in the test rig, structures laboratory, department of civil engineering, Indian institute of science, Bangalore. The geometric details and the AE sensor locations in the test specimen are specified in Table 3. Generally in concrete, micro-cracking starts to develop initially, accompanied by a number of AE hits once it reaches tensile strength. Figure 4 shows a typical recorded load versus time plot, variation of axial strain with load and mid-span (central) deflection with load. It is interesting to note that the steel yielded at 0.002 strain, which confirms the earlier known results and also the maximum deflection at collapse is 14 mm [specimen LL1; depth 450 mm] which agrees with the code of practice IS 456-2000 [26].

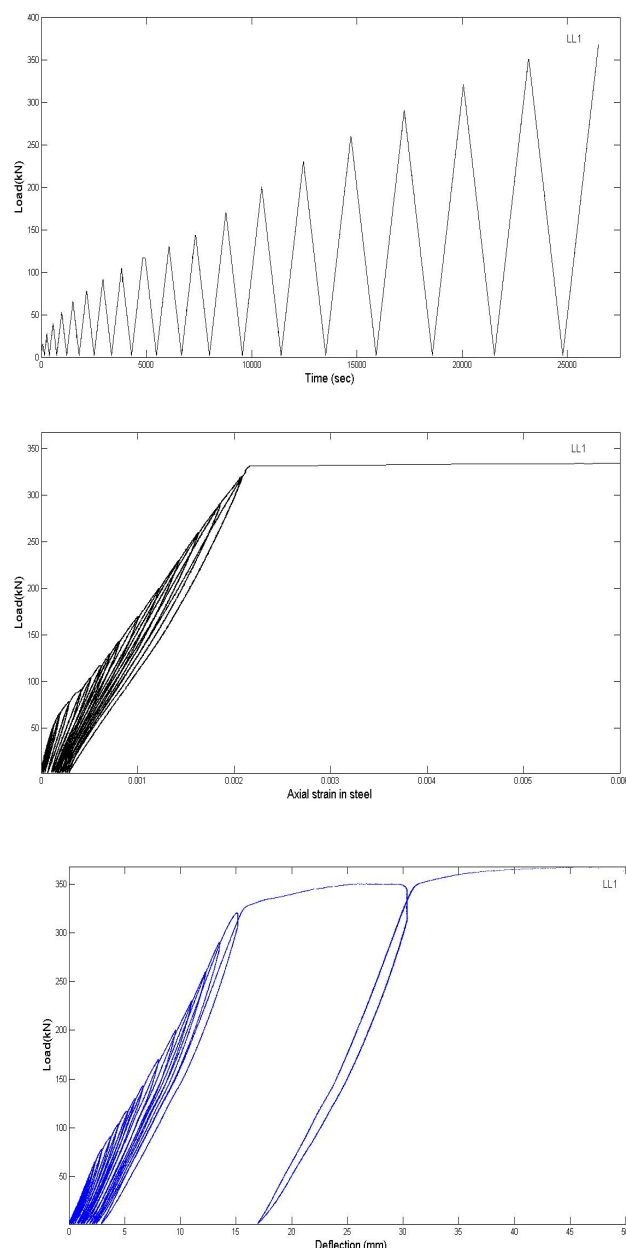


Figure 4. Typical recorded load versus time, axial strain versus load and deflection versus load plots during experiment

Figure 5 shows variation in average frequency (AF) with RA as the fracture progresses in the specimen with load. AF and RA values for each loading cycle for all nine RC specimen were calculated¹¹. When the variation of average AF against RA for each cycle is plotted, as shown in Figure 5, a trend is observed along the depicted curve. AF gradually decreases as the loading progresses. The points of AF versus RA plot in Figure 5

are clustered closely at the final loading cycles compared to earlier loading cycles. This trend was observed for the specimens with depth 450 mm, 300 mm and 150 mm.

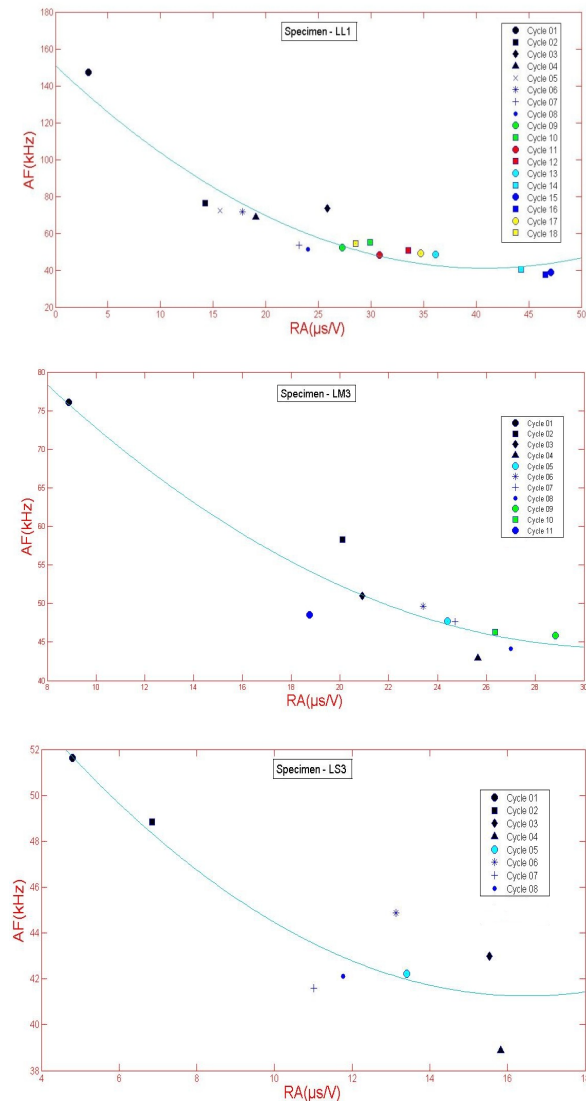


Figure 5 Trend of variation of average frequency (AF) against RA value

It has been observed that, in case of incremental cyclic loading on RC beams with depth 450 mm, as fracture progresses, the average AF value for each cycle decreases gradually, as depicted in Figure 5. Whereas, the value of average RA value of each cycle is observed to be increasing. The same trend was observed in case of beams with depth 300 mm and 150 mm.

The negative slope of the trend line shown in Figure 5 is decreasing as the damage progresses further and eventually comes to zero. The line in Fig.5 shows the trend of the average frequency variation with RA. This trend is same for specimens with depths of 450 mm, 300 mm and 150 mm. The reason could be that the emissions during the early damage stage exhibit higher AF and lower RA. When as the material is led to collapse state AF decreases and RA increases. Also the RA value has been observed to gradually increase with time. The large number of AE data indicates huge range of experimental parameters due to different source locations. It was observed that as the specimen reaches collapse state the points are clustered as compared to the initial loading stage.

Figure 6a depicts the change in AF value, load with time for specimen depth of 450 mm. Average value of AF for each cycle is taken and represented at the corresponding peak load. Figure 6b shows a set of graphs showing the plot of rise time (RT) versus amplitude for each cycle. It is noted that, when there is a steep decrease in AF value from cycle 3 to cycle 4 as shown in Figure 6a, a sudden increase in rise time is observed from cycle 3 to cycle 4 in Figure 6b. This could be due to formation of shear cracks in the specimen [28-31].

A clear difference can be observed from Figure 6b when the plots of first 3 cycles are compared with those of last 3 loading cycles. It can be seen that there is a notable increase in the value of average RT between the first 3 cycles and last 3 cycles. This clearly indicates a distinction between formation of tensile cracks and shear cracks in the specimen. During the first 3 loading cycles, tensile cracks occur, which produce AE hits of shorter rise time. For the last 3 loading cycles, shear cracks are observed, which produce AE hits with longer rise time. It could be possible to find a correlation between AE parameters like average frequency and rise time.

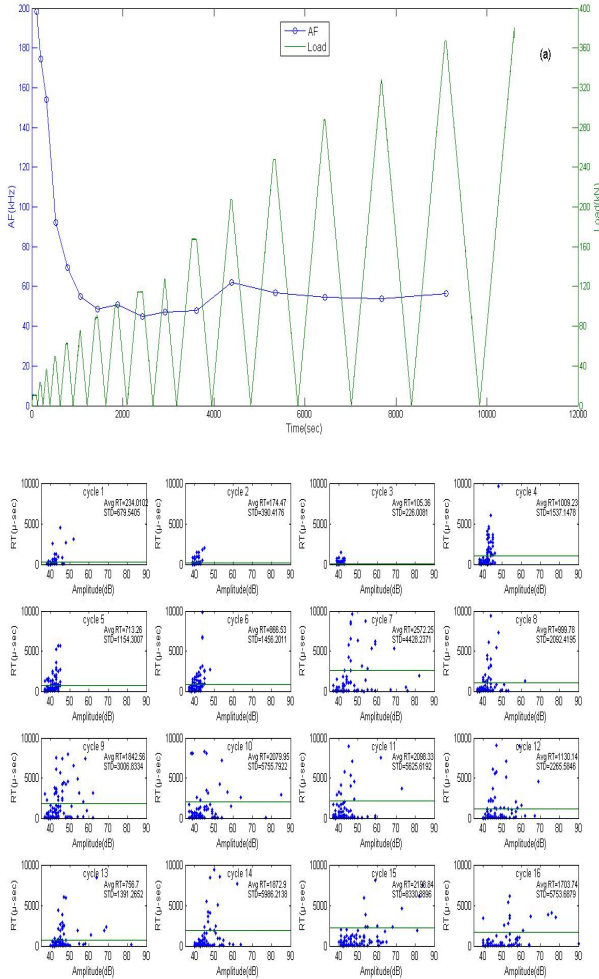


Figure 6 (a) variation of AF and load with time (b) the corresponding plot of rise time versus amplitude for each cycle [specimen depth is 450 mm]

In Figure 7, It has also been observed that the maximum RMS of voltage increases significantly as the specimen reaches failure. It is seen that the maximum RMS of failure cycle is approximately 10 times more than that of the 1st cycle. This concludes that beam failure can be predicted by observing the value of maximum RMS.

There is a rise in the maximum value of RMS before collapse which indicates the structure nearing its failure. It was observed that there is a significant increase in the maximum RMS value from cycle 10 to cycle 11. It can be said that maximum RMS parameter can effectively be used in monitoring damage in RC structures. It was observed that once the steel

reached above its elastic strain, the slope of line plotted between AF and time became zero. It was observed that RA increases with time and when the permanent strain in steel is present the RA value has reached approximately a constant value.

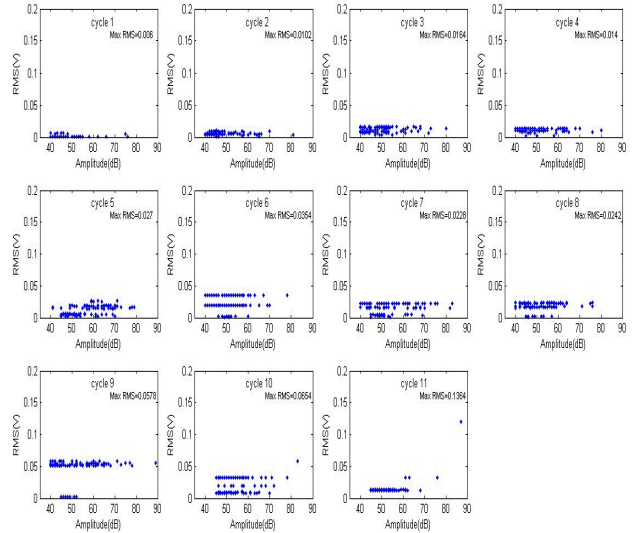


Figure 7 plot between RMS versus amplitude for each cycle [specimen depth is 300 mm]

5.1 AE based *b*-value analysis

The AE- based *b*-values were computed for each cycle [22]. The total number of AE hits was divided into groups. The cumulative number of AE hits in steps of 5dB was calculated. A graph was plotted between the logarithm of cumulative AE hits and amplitude (dB/20). The least square method of curve-fitting was adopted to get a linear trend. The negative slope of the line is the *b*-value [22]. It was observed that there was not much variation in the trend of *b*-values due to the change in the group size of 100 AE hits. It was observed that *b*- values of groups of 100 AE hits fall between the groups for 70 hits and 150 hits, hence groups of 100 AE-hits are taken for further *b*-value analysis.

In each loading cycle, the b -value reaches its minimum and is more clustered during the peak load of the corresponding cycle. At the region after the peak load, the b -values tend to increase and appear more scattered. This trend is noted in all the loading cycles. As the load increases the b -value is fluctuating. When the maximum previous load is reached as sharp drop is recorded. A local minimum of the b -value is found at the maximum load of the cycle.

The fluctuations are more and the b -values are more clustered were observed only after the peak load in the previous load cycle was attained. This could be due to the presence of Kaiser effect in concrete structures. Kaiser is defined as AE are not observed during the reloading of a material until the load exceeds its previous peak load [5]. Moreover, the minimum b -value at the peak loading showed a decreasing trend as the peak load intensity increased for each cycle. The lowest b -value was reached at the peak of final loading cycle, indicating the damage state of the structure. The clustering of the b -value during the peak load is due to the micro-crack formation in the structure. The increase and the scattering of b -values after the peak load is attributed to the micro-crack growth is proceeding. The decreasing trend of the b -value with the progress in the loading cycle depicts the micro-crack localization leading to macro-crack. When the b -value reaches its least, it can be interpreted that the structure is severely damaged. Also, the maximum b -values noticed after the peak load showed a decreasing trend as the loading cycles progressed. This may be due to the micro-crack growth.

5.2 Damage Parameter (D)

The damage parameter (D) was computed by considering a group of 100 AE hits [23]. It was observed that the damage parameter (D) reached maximum at peak load of each loading cycle. Interestingly, the b -value also reached its minimum at the same point. As peak load increased in each cycle, the damage parameter (D) also increased. During the last loading cycle, the damage parameter (D) reached its maximum value. This shows that the beam experiences maximum damage at the

loading maximum. b -value is least when the beam is nearing collapse.

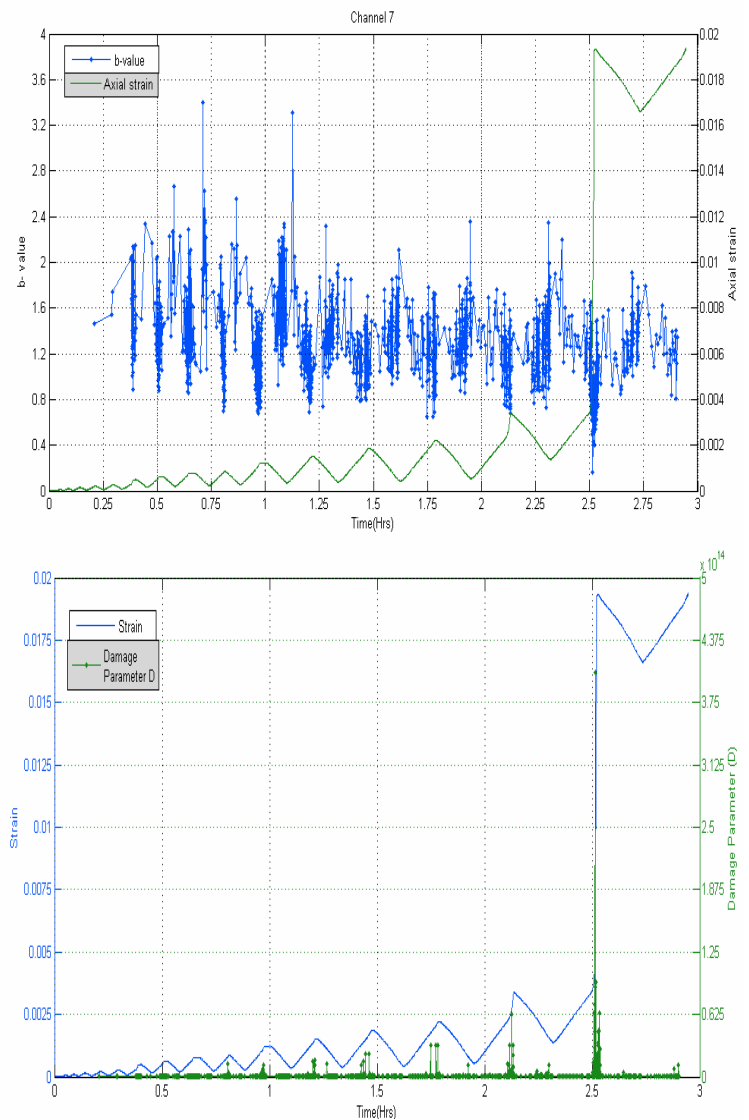


Figure 8. Variation of AE based b -value and damage parameter with axial strain in steel

Figure 8 shows the variation of AE based b -value and damage parameter (D) with axial strain in the steel. The strain in steel is recovered during the end of initial cycles showing that the structure was in elastic state. From the 7th loading cycle onwards, there was permanent strain in steel, indicating that the structure had undergone a permanent deformation. Also, the trend in b -value variation started at this loading cycle. It can be noted that the b -value reached minimum when the strain reached maximum. On the other hand when the strain was at its minimum, the

b -value reached maximum. The b -value reached its minimum at the collapse state of the specimen. During the yielding, large amount of AE signals are released due to formation of macro-cracks, due to this reason there is decrease in b -value. From Figure 8, It was observed that the damage parameter increased each time there is an increase in axial strain, and it reached maximum when the steel yielded. This shows that b -value and damage parameter (D), reciprocates the damage state of the structure.

6. MICRO-CRACKING ACTIVITY AS INFERRED FROM AE STATISTICS IN PLAIN CONCRETE

The recorded AE data files were replayed and processed using AE^{win} SAMOS software for the identification and evaluation of various phases of fracture process using the data of AE event counts (n), energy (E) counts and amplitude distribution data at the maximum possible digitization rate of 200 bin resolution. The frequency of occurrence of micro-cracking activity has been studied using the event rate $\left(\frac{dn}{dt}\right)$ and energy count rate $\left(\frac{dE}{dt}\right)$ data plots. The AE cumulative energy count data ($\sum E$) were normalized with respect to the final energy count for obtaining the normalized micro-crack damage data of the tested specimens following the procedure reported in detail elsewhere[32]. The origin and development of micro-cracking activity in cement concrete as well as in mortar can be inferred from AE statistics, as the number of AE events is more or less proportional to the number of growing cracks and the AE amplitude or energy count data are proportional to the crack growth increments in brittle and quasi-brittle materials like rock and concrete. The most useful AE statistical parameters to identify and characterize the various stages of micro-cracking activity in concrete are: (i) The occurrence rate of event and energy counts, (ii) Amplitude distribution (b -value) and its stress-induced changes, and (iii) Cumulative energy or event counts. The

results of the present study show that micro-cracking activity occurs in three successive stages, namely, Initiation (I), Coalescence (C) and Nucleation (N) that would lead to the final failure of concrete as well as mortar specimens under bending stress. In fact, the formation of micro-cracks is ubiquitous in brittle and quasibrittle materials at stresses close to the yielding point. The micro-cracking activity can be controlled during the initiation and coalescence stages. The statistics of AE occurring during these phases are distinctly different for both cement concrete and mortar as shown in Figure 9.

6.1 Frequency of occurrence

The AE event rate refers to the frequency of occurrence of micro-cracking activity while the energy or peak amplitude corresponding to the individual AE events represents the size of micro-crack or its incremental growth in brittle and quasibrittle materials. The rate at which AE energy is released is a measure of size distribution of micro-cracks in all such materials. Initially as loading commenced, hardly any AE activity (energy per event or ring down count) was observed. With the formation of new micro-cracks, the specimens began to generate AE which increased steadily. The formation of AE (or micro-cracks) commenced at 140 sec after the start of the experiment for concrete specimen (78 Mpa), at 120 sec for (50 Mpa) concrete specimen and rather early at 90 sec after start of the experiment for mortar specimen as shown in Figure 9.

By replaying the AE data recorded, the log of energy release rate versus time and log of event rate versus time plots for both concrete and mortar specimens are obtained and these are shown in Figure 9. From these plots it can be seen that the trend in AE energy release rate versus time and AE event rate versus time is more or less remain similar in all the specimens. The AE increased steadily with increase of load indicating the formation and growth of micro-cracks and continued further after the peak load is attained upto nearly 450 sec from the start of the experiment in concrete specimen as shown in Figs 9a and 9b and upto 300 sec in mortar specimen shown in Fig. 9c.

Region-I called initiation phase showing raising trend, region-II called coalescence phase which has a constant trend and the region-III called the nucleation phase which shows a decreasing trend. The initiation phase (I) is the steady increase in both the parameters which indicates the formation of new micro-cracks during the prepeak load and post peak load regimes can be termed as initiation phase (I) of micro-crack damage in concrete. It is then followed by coalescence (C) and nucleation phase (N) of micro-crack damage in concrete. The coalescence phase (C) is characterized by nearly stable or with minor fluctuations in the plot. It can be attributed to subcritical growth of micro-cracks. The nucleation phase (N) is characterized by a gradual decrease in both the parameters indicating the progress towards final failure due to aggregate interlock and frictional effects. Coalescence phase is a combined process involving activities such as micro-crack deflection, aggregate bridging and crack face friction. These plots may be useful in identifying the various phases of micro-crack damage during the failure of concrete.

Micro-crack density distribution represents the number of micro-cracks per unit of observation area. It was observed that the fluctuations of were more in case of the mortar specimen when compared to that in concrete specimens. This indicates that the density and size distribution of micro-cracks in concrete specimens is more or less uniform and small. While in case of mortar specimen, the fluctuations as seen in the plot are relatively high indicating that the density and size distribution of the newly formed micro-cracks can be non-uniform and larger in size.

It is interesting to see from Figure 9 that the mortar specimens which have a low compressive strength (~ 47 MPa) showed more frequent fluctuations. The concrete specimen (mix-F: 78MPa) showed the least amount of fluctuations. The concrete specimen (mix-B: 50 Mpa) showed fluctuations somewhere in between. The reasons for the changes in fluctuations in addition to the compositional and preparation differences could be many. (i) Ultrasonic attenuation form

AE source to the sensor (receiver) could be varying the measured AE energy. (ii) In view of ultrasonic wave propagation, the size of the largest aggregates approaches that of the shortest wave length. Also there is attenuation caused by material absorption. All these factors cause significant reduction in the total energy of AE waves reaching transducers. The two basic quantities which describe a sound wave are the frequency n , of the wave and the wavelength, λ . These quantities are related to each other and to the velocity of sound wave (V) by a well known relation $v=n\lambda$, where V is velocity of sound in concrete in m/sec, n is frequency, kHz and λ is wave length in mm.

In the present study 3800 m/sec was used as sound velocity in concrete. A wavelength of 20 mm would correspond to a frequency of 190 kHz and this frequency is with in the range of 100 kHz - 500 kHz. In general for concrete AE signals are emitted with in the range of 100 kHz - 500 kHz. In the present study the maximum aggregate size is 20 mm. Therefore it scattering of ultrasonic waves. If the wave length is less than size of aggregate then there is higher probability of internal reflection of the waves, which is called scattering. This scattering may absorb energy. The ultrasonic scattering causes additional signal AE wave attenuation. Since concrete is known to be a highly attenuating material, lower frequency sensors are suitable. The available sensor though has a highest sensitivity between 35 kHz - 100 kHz, it is still able to pickup the signals with frequency higher than 100 kHz. Since the maximum aggregate size in concrete is 20 mm, the wavelength should be greater than 20 mm. Accordingly, using the relation $V=n\lambda$ the frequency of the AE sensor to be used is desirable to be less than 190 kHz. Accordingly R6D sensor which has a highest sensitivity in the range 35 kHz – 100 kHz has been used. However there is surely ultrasonic attenuation in mortar specimens. But when compared to concrete specimens the effect of scattering is less evident than that of concrete with large size coarse aggregates.

RDC and energy counts have the same

trend in three phases. It is less in the initiation phase and nucleation phase while it is large in the coalescence phase.

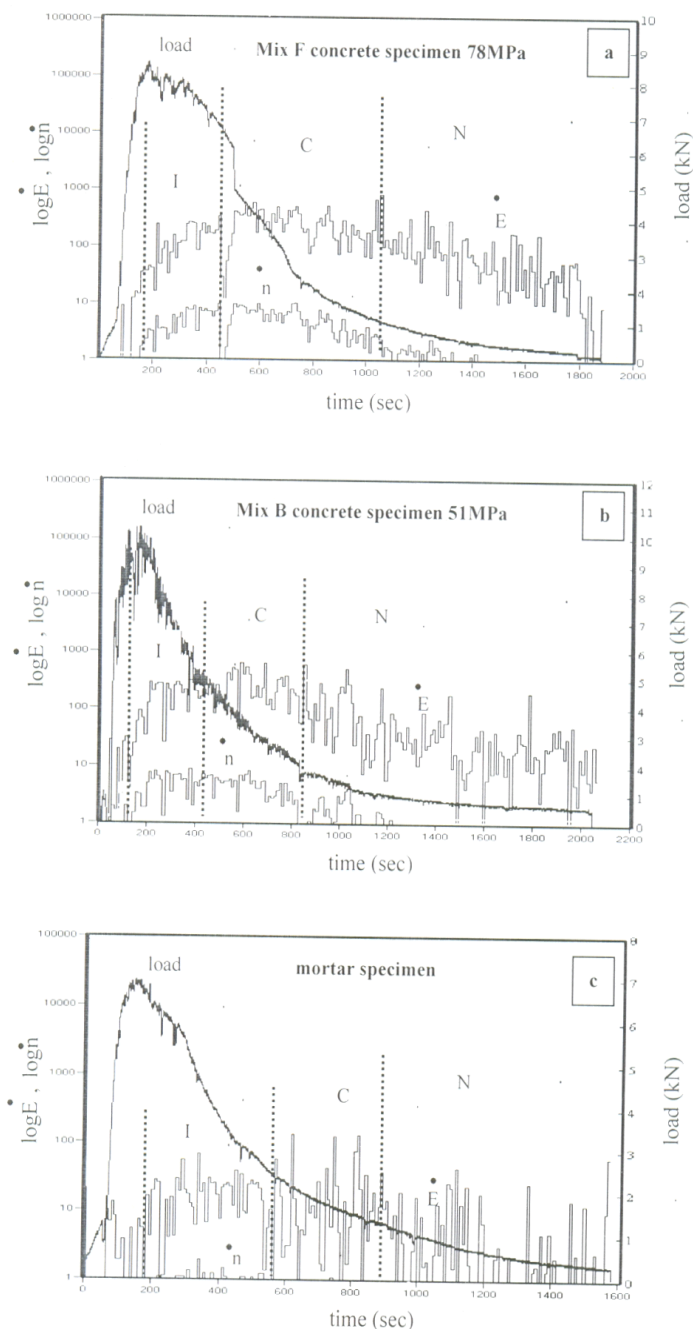


Figure 9. The logarithm of AE event (n) and AE energy count (E) data obtained during the experiments on (a) concrete specimen [high strength], (b) concrete specimen [low strength] and (c) mortar specimen plotted against time. The load versus time plots are also included in the Figure 9.

Interestingly $\frac{E}{n}$ continues to increase from

initiation phase to nucleation phase. It was observed that micro-cracking during nucleation phase (N) was more intense in concrete specimen (78Mpa) while the micro-crack accumulation in the other concrete specimen (50Mpa) was found to be more intense at an early stage of the coalescence (C) phase which is signified by the E/n ratio. Hence it can be inferred that as the strength decreases, damage occurs at an early stage. Also, micro-cracking in mortar specimen had suddenly increased during nucleation phase.

The above results may be useful for the classification of cracks in RC beams and plain concrete beams with the help of AE parameters such as average frequency, amplitude, rise time and RMS and RA. It will be interesting if comparison is made between mechanical measurements such as strain in concrete and central deflection of the beam with the AE parameters.

7. CONCLUSIONS

1. Tensile cracks are developed at the initial stage of loading, while shear cracks dominate later. Variation in RT with amplitude indicate the type of the crack.
2. The RMS voltage of AE signal is useful for recognition of approaching failure of the specimens. Changes in AF and RT values are characteristic of the damage state of the structure.
3. b -value analysis is useful for identifying the micro-crack or macro-cracks in structure. The variation of damage parameter (D) and b -value indicates the damage state of the structure.
4. The trends of $\log E$ and $\log n$ of AE versus time are quite useful to identify and analyze various stages of micro-cracking activity in the samples tested. Micro-cracking occurred in three different successive phases namely initiation, coalescence and nucleation in both concrete and mortar specimens.
5. Both concrete and mortar test specimens have shown similar trends with regard to the changes in RDC and energy count data of AE during the course of the experiments. The results have helped in identifying the crack initiation and crack damage states for the samples tested.

Table 1. Geometric details of the RC beam test specimens

Specimen	Ø(mm)	n	A _s (mm ²)	L (mm)	S(mm)	b (mm)	D (mm)	ρ(%)	a/d	P _u (kN)
LL1	20	3	943	3200	3000	150	450	1.396	2.0	367.4
LL2	20	3	943	3200	3000	150	450	1.396	2.0	330.0
LL3	20	3	943	3200	3000	150	450	1.396	2.0	382.9
LM1	20	2	628	3200	3000	150	300	1.395	3.34	130.9
LM2	20	2	628	3200	3000	150	300	1.395	3.34	132.8
LM3	20	2	628	3200	3000	150	300	1.395	3.0	135.3
LS1	12	3	339	3200	3000	150	150	1.506	6.0	25.5
LS2	12	3	339	3200	3000	150	150	1.506	6.0	25.9
LS3	12	3	339	3200	3000	150	150	1.506	6.0	27.8

Ø=nominal diameter of reinforcement; n=number of reinforcement bars; A_s= area of reinforcement; L=beam length; S=Span of the beam; b=beam width; D= Beam depth; ρ=%of reinforcement; a/d=ratio of shear span to depth; P_u= final failure load;

Table 2: Concrete mix details for RC beams

Property	Concrete mix
Water/cement ratio	0.51
Cement, kg/m ³	313.2
Fine aggregate, kg/m ³	488.0
Coarse aggregate, kg/m ³	1240.7
Water, kg/m ³	161.4
Compressive strength (28-days), N/mm ²	58.0
Tensile strength, N/mm ²	3.5

Table 3: Sensor's locations on the RC beam test specimen

D = 450 mm	Sensor No.	Sensor Location		D=300 mm	Sensor No.	Sensor Location		D=150 mm	Sensor No.	Sensor Location	
		X	Y			X	Y			X	Y
LL1	1	1200	397	LM1	1	2395	245	LS1	1	735	50
	3	1200	100		2	2395	25		3	1200	75
	5	2000	100		4	2600	145		5	1800	110
	7	2000	397		5	800	272		7	2500	40
LL2	1	1200	397	LM2	7	795	25	LS2	1	480	120
	3	1200	100		8	440	140		3	1200	75
	5	2000	100		4	1900	250		5	1800	110
	7	2000	397		5	1900	50		7	2500	40
LL3	1	1200	397	LM3	7	1100	250	LS3	1	480	120
	3	1200	100		8	1100	50		3	1200	75
	5	2000	100		1	1200	100		5	1800	110
	7	2000	397		3	2000	100		7	2500	40
					5	1200	273				
					7	2000	273				

REFERENCES

- [1] Van Mier, J.G.M., 1997. *Fracture Processes of Concrete*. CRC Press.
- [2] Karihaloo B.L., 1995. *Fracture mechanics and structural concrete*. Longman Scientific & Technical, New York.
- [3] Shah, S.P., Swartz, S.E. and Ouyang, C., 1995. *Fracture mechanics of concrete: Applications of fracture mechanics to concrete, rock and other quasi-brittle materials.* John Wiley & Sons, Inc, New York.
- [4] Bazant, Z.P. and Planas J., 1998. *Fracture and size effect in concrete and other quasi brittle materials*. CRC press, Boca Raton, FL.
- [5] Grosse C.U., Ohtsu M. 2008. *Acoustic Emission Testing*. Springer, Heidelberg.
- [6] R.Vidya Sagar, B.K.Raghu Prasad. 2012. A Review of recent development in parametric based acoustic emission techniques applied to concrete structures, *Nondest test and eval*, **27**:47-68.
- [7] Mindess S., 2004. Acoustic emission methods. In: *CRC Handbook of Nondestructive Testing of Concrete* (Malhotra V. M., Carino N. J. (Ed.)). CRC, Boca Raton, FL.
- [8] Chang P. C. and Liu S. C., 2003. Recent research in nondestructive evaluation of civil infrastructures. *J Mat in Civil Eng*. **15**: 298-304.
- [9] JCMS-IIIB5706, Monitoring method for active cracks in concrete by acoustic emission, Construction Materials Standard, *Federation of Construction Materials Industries, Tokyo, Japan, 2003*.
- [10] Ohtsu M., 2010. Recommendations of RILEM Technical Committee 212-ACD: acoustic emission and related NDE techniques for crack detection and damage evaluation in concrete: 3. Test method for classification of active cracks in concrete structures by acoustic emission. *Mat and Str*. **43**:1187–1189.
- [11]. Dimistrios G. Aggelis., 2011. Classification of cracking mode in concrete by acoustic emission parameters *Mech Res Com*, **38**:153-157.
- [12]. Ohno K. and Ohtsu M., 2010. Crack classification in concrete based on acoustic emission. *Cons and Build Mat*. **24**., 2339–2346.
- [13]. Ohtsu M., Tomoda Y., 2007. Phenomenological model of corrosion process in reinforced concrete identified by acoustic emission. *ACI Mat J*. **105**: 194–200.
- [14]. Polyzos D., Papacharalambopoulos A., Shiotani T. and Aggelis D.G. Dependence of AE parameters on the propagation distance. In: *Progress in Acoustic Emission XV* (Wakayama, et al. (Eds.)), 2010, pp. 43–48.
- [15]. Richter Charles, F. *Elementary Seismology*, W.H Freeman and company San Francisco and London, 1958.
- [16]. Gutenberg, B. and Richter, C.F. *Seismicity of the Earth and Associated Phenomena*. Princeton University Press. Princeton, NJ., USA, 2nd edition, 1954.
- [18]. Main I. G., 1991. A modified Griffith criterion for the evolution of damage with a fractal distribution of crack lengths: Application to seismic event rates and *b*-values. *Geophy J Int*, **107**:353- 362.
- [19]. Turcotte D. L., Newman W.L. and

- Shcherbakov R. 2003. Micro and macroscopic models of rock fracture. *Geophy Int J*, **152**:712-28.
- [20]. Carpinteri A., Lacidogna G. and Puzzi S. From criticality to final collapse: Evolution of b - value 1.5 to 1.0., 2009. *Chaos, Solit and Fract.* **41**, 843-853.
- [21]. Rao, M.V.M.S. and Prasanna Lakshmi, K. J., 2005. Analysis of b -value and improved b -value of acoustic emissions accompanying rock fracture. *Cur Sci*, **89**:1577-1582.
- [22]. Colombo, I.S., Main, I.G., and Forde, M.C., 2003. Assessing damage of reinforced concrete beam using b -value analysis of Acoustic emission signals. *J Mat in Civil Eng.* **15**:280-286.
- [23]. Cox, S.J.D and Meridith, P.G., 1983. Microcracking formation and material softening in rock measured by monitoring acoustic emissions, International Journal of Rock Mechanics. *Min Sci & Geomech. Abst*, **30**:11-24.
- [24]. Ohtsu M, Ono K., 1984. A generalized theory of acoustic emission and Green's functions in a half space. *J acou emis*, **3**:124-33.
- [25]. Ohno K, Ohtsu M. Mechanisms of concrete fracture analyzed by AE-SiGMA with automatic detector of first motion. In: Proceedings of international conference on fracture; 2008 [in CD-ROM].
- [26]. Indian standard code of practice for plain and reinforced concrete, IS 456: 2000, Fourth Revision, Bureau of Indian Standards, New Delhi, 2002
- [27]. Aggelis, D.G., Matikas, T.E., Shiotani, T. Advanced acoustic techniques for health monitoring of concrete structures. In: The Song's Handbook of Concrete Durability (KIM S.H., ANN K.Y. (Eds.)). Middleton Publishing Inc. 2010b pp. 331-378.
- [28]. Aggelis D.G., Shiotani T., Momoki S. and Hirama A., 2009. Acoustic emission and ultrasound for damage characterization of concrete elements. *ACI Mat. J.* **106**:509-514.
- [29]. Aggelis D.G., Shiotani T. and Terazawa M., 2010. Assessment of construction joint effect in full-scale concrete beams by acoustic emission activity. *J Eng Mech.* **136**:906-912.
- [30]. Curtis G. J. 1975. Acoustic emission energy relates to bond strength. *Non-Des. Test.* **8**: 249-257.
- [31]. Shitani T., Aggelis D.G. and Makishima O., 2009. Global monitoring of large concrete structures using acoustic emission and ultrasonic techniques: case study. *J Bridge Eng.* **14**:188-192.
- [32] Rao MVMS, Prasanna Lakshmi KJ, Nagaraja Rao GM, Vijayakumar K, Udayakumar S., 2011. Precursory microcracking and brittle failure of Latur basalt and migmatite gneiss under compressive loading. *Cur Sci* **101**:1053-1059.